CFD MODELLING OF A SUBTERRANEAN BUSBAR FOR THERMAL PERFORMANCE

[1]Andrew CAMPBELL, [1]Madhat ABDEL-JAWAD, [2]Steve APPLEBY, and [3]Guillaume SERVANT

[1]WorleyParsons, Level 12 333 Collins St, Melbourne VIC 3000 Australia

[2]WorleyParsons, Level 5 Focus Five Building 23 - 31 Gheringhap Street Geelong VIC 3220 Australia

[3]Tomago Aluminium, PO Box 405 Raymond Terrace NSW 2324 Australia

ABSTRACT

Aluminium smelters rely on the transmission of large electrical currents to provide power for the smelting process for each pot. The transmission of electrical energy is generally achieved using subterranean busbars, which are large (~0.5 m^2 cross sectional area and tens of meters in length) aluminium electrical conductors. The process of electrical conduction through these busbars also results in the generation of significant amount of heat due to which the failure to effectively cool a busbar can result in high temperatures and subsequent catastrophic failure for a smelter. WorleyParsons Advanced Analysis Group undertook modelling for Tomago Aluminium to investigate Busbar temperatures at increased operational electrical currents. The model which included the multiphysics of flow, free convection, buoyancy and thermal conduction through the busbars was undertaken using a commercial finite volume solver. The current conditions for the operation of the busbar were examined and compared with on-site measurements and proposed alternatives were also investigated.

NOMENCLATURE

a   characteristic length
p   pressure
u   velocity
ρ density
μ dynamic viscosity

INTRODUCTION

Aluminium is produced at Tomago by the electrolysis of alumina using the Hall-Héroult process. This process involves the solution of Alumina in molten cryolite, which has a melting point lower than that of Alumina.

The electrolysis of the solution results in the precipitation of liquid aluminium at the cathode. The liquid Aluminium sinks to the bottom of the pot and is siphoned out using a method called single ladle direct tapping. The components are electrically heated and the pots are continually replenished hence a continuous supply of considerable electrical energy is required for the process. This is delivered using large heavy cast aluminium busbars connecting the pots in a potline.

A large current is drawn by each pot and the busbar dissipates a significant amount of energy due to resistive heating.

As in most Aluminium smelters, the arrangement of the Pots is in the form of two parallel lines of Pots ("Potrooms") linked at one end by the power supply and

at the other end by an interconnecting busbar referred to as the "Crossover Busbar". This complete arrangement is called a Potline. To allow free movement of equipment into the area between the Potrooms it is common practice to place the Crossover Busbar under ground in a ventilated tunnel. In the case of the Tomago plant, the tunnel is open at each end and has a small vent located midway along its length. Air moves due to natural/free convection heating the air in the tunnel that then escapes through the vent.

Little is available in the open literature on prior work on CFD of busbars in tunnels. To the best of our knowledge this is the first published computational work on the topic. Some published work exists on broadly related methodology. [1-4]

Tomago Aluminium is conducting a study to investigate the implications of an increase in Line Current from 228kA to 240kA. One aspect of this change is an increase in heat generation in Crossover Busbar. Without management this additional thermal load can have a mechanical loading impact brought about by busbar temperature rise and associated thermal expansion. To support Tomago's investigation, WorleyParsons was engaged to establish what temperature changes would occur with the increased current and to develop solutions to control the temperature rise. WorleyParsons, Melbourne Advanced Analysis Group, undertook to develop CFD models for the baseline case and several other options.

Three geometric configurations of the tunnel busbar were examined and are listed in Table 1 whilst the geometry of the aluminium busbar was identical for all cases. The system was modelled for 2 currents (228kA and 240kA) for the existing setup and the proposed modifications were modelled at the increased current.

Table 1: Matrix of cases modelled.

Case	Geometry	Current (kA)
1	Existing case	228
2	Existing case	240
3	Addition of 7 m tall cylindrical stack	240
4	Addition of 3 Flat Roof Vents to tunnel	240

MODEL SETUP

General Description

The model comprised of the Navier-Stokes equations implemented using a commercial Navier-Stokes solver.

The k-ε turbulence model was implemented. The heat was generated in the solid aluminium bar according to the power (I^2R) where the resistance R is calculated from the resistivity as a function of the temperature using equations 1-4.

The model included convective (solid-gas) heat transfer as well as conduction through the solids. The commercial finite volume solver used (ANSYS CFX) allows the coupling of both heat transfer mechanisms with the Navier Stokes equations. All equations along with the turbulence model were solved simultaneously. The coupled CFD model includes two materials: Air and Aluminium (solid).

The model included convective (solid-gas) heat transfer as well as conduction through the solids. Heat generation within the busbar was modelled as a source calculated based on the current passing through the busbar and the resistivity of the busbars [5]. A symmetry plane across the solid and air domains was exploited in all calculations in order to reduce computational times and shown in Figure 1. Calculations were carried on a commercial finite volume solver (CFX).

Mesh sizes ranged from 200,000 to 800,000 nodes with the main bulk parameters (taken as the bulk gas average temperature and the busbar average and maximum temperatures) varying only slightly between the smallest and the largest mesh.

Steady state simulations were run with buoyancy accounted for and with an automatic time step of the order of 0.01s. Simulations were run till the residuals dropped by four orders of magnitudes and imbalances were negligible.

Some geometric details of minor significance to the physics of the problem were simplified out from the model. The busbars were modelled with no supports as shown in Figure 2 as the influence of these is expected to be minimal. The modelled section of the tunnel was therefore 25 m long with cross sectional dimensions as shown in Figure 3.
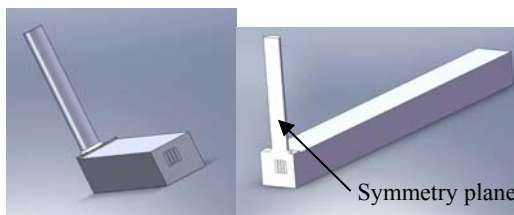

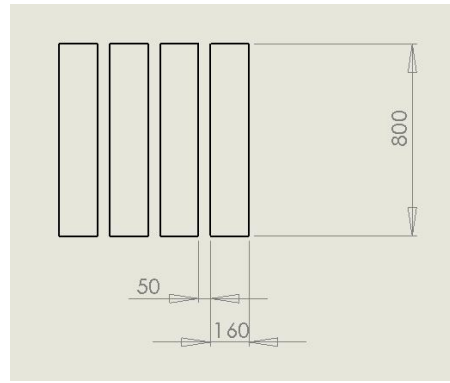**Figure 1:** Schematic of the tunnel and busbar system showing the symmetry plane.

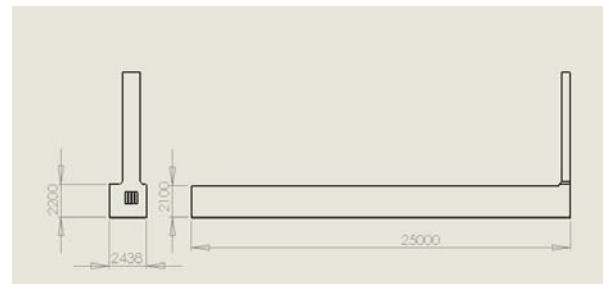**Figure 2:** Dimensioned front view of the bars.

Figure 3: Dimensioned side view of the tunnel (stack scenario).

MATERIAL PROPERTIES

The CFX properties for Aluminium and Air (Ideal Gas) were used in this modelling. The key values are summarized in Table 2.

Resistivity, ρ, for 1350 grade Aluminium provided [6] is

$$\rho = 0.0283 \times (1 + 0.00405 \times (T - 20)) \qquad \mathbf{1}$$

Where   ρ is given in μΩ.m,
                  T is given in ºC.

Table 2: Summary of Key Property values Used

Material	Property	Value
Aluminium	Density ρ (kg/m³)	2702
	Specific Heat C_p (J/kg.K)	903
	Thermal Conductivity k (W/m.K)	237
Air, Ideal Gas	Molecular Weight M (kg/kmol)	28.96
	Specific Heat C_p (J/kg.K)	1004.4
	Thermal Conductivity k (W/m.K)	0.0261
	Dynamic Viscosity μ (Pa.s)	1.831e-5

Boundary Conditions

The boundaries were set up using the conditions in Table 3.

Table 3: Boundary Condition Summary

Boundary & Type	Parameter	Condition
Inlet (Opening)	Flow Pressure Condition	P = Pneumatic head
	Thermal (for Inflow)	T = 60 ºC
Outlet (Opening)	Flow Pressure Condition	P = Pneumatic head
	Thermal (for Inflow)	T = 25 ºC
Symmetry Plane	Flow	Effectively a Wall
	Heat Transfer	Effectively Adiabatic
Tunnel Wall	Flow	Non Slip Wall
	Heat Transfer	Adiabatic

For the opening pressure boundary conditions, a pneumatic head is calculated and applied based on equation 2.

$$P_{opening} = \rho g (2 - x) \qquad \textbf{2}$$

Where   x is in the vertical direction (m)
ρ is the average density at the opening conditions for air (kg/m^3).

Heat Source

The total heat source across the busbar was calculated due to the current flowing through it using equation 3.

$$P = I^2 R \qquad \textbf{3}$$

Where   P is Power in Watts (W)
I is the Current in Amps (A)
R is the resistance in Ohms (Ω)

Resistivity is calculated using equation 4

$$R = \rho \frac{l}{A} \qquad \textbf{4}$$

Where   l is length of the conductor (m) – and is 25m in this instance
A is the cross sectional current flow path (m^2) – and is 0.5120m^2

Assuming T = 120 ºC
$$\Rightarrow \rho = 0.0283 \times (1 + 0.00405 \times (120 - 20))$$
$$= 3.976 \times 10^{-8}\ \Omega m$$

Assuming I = 228kA
$$P = I^2 R$$
$$= (228 x 10^3) \times 3.976 \times 10^{-8} \times \frac{25}{0.5120}$$
$$= 100926\ W$$
$$= 101\ kW$$

The resistivity, a function of temperature, was used to calculate the resistance R by (4). The power dissipated into heat was then given by the product of the resistance and square of the current I^{2}R. The total power calculated was found to be in good agreement with measured data to within 5%.

The heat source is applied across the busbar volume using the power calculated by an expression following this method. As the current is constant for each case, the local heat source is dependent on temperature due to the temperature dependence of the resistivity.

RESULTS

The main metric of performance of the cooling system is the temperature field of the busbar. The results for the baseline air velocities and temperatures were similar to the measured plant data. The normalised temperature field results are shown in below in figures 4-7 for a uniform scale. As expected the hottest portions of the bars for the existing case is away from both ends of the tunnel However, there are significant differences between the temperatures of the different configurations which are all normalised by a value slightly exceeding the maximum temperature for case 2.

The main metrics of the runs (with the temperatures normalised) are summarized in table 5 below. It is noteworthy that the volumetric flow rate of air is significantly increased by the geometry modifications.

Table 4: Summary of simulated results

Case	Current (kA)	Busbar Temp Mean (Norm)	Busbar Temp Max (Norm)	Outlet Air Velocity (m/s)	Outlet Air Temp (ºC)
1	228	0.62	0.96	7.6	83
2	240	0.65	0.98	7.64	95
3	240	0.62	0.73	11.2	71
4	240	0.40	0.49	3.2	64

The increase in current between cases 1 and 2 is about 5%, the increase in power dissipation is proportional to the current squared therefore it was anticipated that the results for cases 1 and 2 would be within about 10% of each other. The volume fraction of the busbar that is at the elevated temperature is greater for the 240 kA case compared with the 228kA case. For example the volume at 0.8 of the maximum temperature or above is approximately 50% greater for the 240 kA case compared with the 228kA case.

The results shown in the figures 6 and 7 indicate that both the geometric modifications are effective in reducing the average and maximum temperatures in the bars. The maximum normalised temperature for case 3 (Figure 6) was significantly reduced to 0.73 indicating that the stack solution would reduce the maximum temperature of the bars at the modelled condition, below the current measured conditions.

The percentage of the busbar volume at normalised temperatures above 0.6 and 0.8 are shown in Table 5 below.

Table 5: Percentage of busbar volumes at temperatures above 0.6 and 0.8 of the normalisation temperature.

Case	Geometry	% volume above 0.6	% volume above 0.8
1	Existing case	46.0	29.6
2	Existing case	46.9	40.3
3	Addition of 7 m tall cylindrical stack	68.1	0
4	Addition of 3 Flat Roof Vents to tunnel	0	0

The results for case 4 (the geometrical configuration with three Flat Roof Vents) shown in Figure 7 indicated that this geometry was the most effective cooling configuration. The maximum temperature in case 4 was slightly lower than the temperature of the outer bar measured for the current configuration (case 1), and nearly half its maximum temperature. Clearly case 4, by allowing a larger volume of air to pass through the tunnel maintains the bars at the lowest temperature.

The results as well as the uniformity of temperature can be attributed to a significant flow rate increase in the two modified cases. The flow rate for the stack case is more than double the original configuration while that for the awning is nearly an order of magnitude greater. This results in significant cooling of the bars which in turn causes a drop in the resistivity and therefore the resistance (according to eq. 1) which results in less heat being generated in the bars compounding the cooling effect.

The Flat Roof Vent option has been predicted to emit air at nominally 64 ºC however the modelling also predicted that the air flow into the tunnel from the basement is increased by a factor of ten (10). The basement air temperature was assumed to be maintained at 60 ºC regardless of air flow however, considering the dramatic increase in air flow, it is considered that the basement air temperature would drop and this would be reflected in a similar drop in the air temperature exhausting from the Flat Roof Vent. This of course would also lead to a further reduction in busbar temperature.

Figure 8 shows the vectors for velocity through the tunnel for the original configuration case. It can be see that the bulk of the flow enters upstream and leaves out through the stack. However it can also be seen that there is a significant portion of the flow at the top of the opening upstream which leaves the tunnel rather than enters. This indicates that the size of the stack opening at the end of the tunnel is insufficient to relieve the pressure gradient setup by the difference in hydrostatic pressure for this stack. Interestingly it is also noted that the bulk of the flow is in the axial direction of the bars this is particularly true in between the bars as can be seen from the figure. The reverse flow for one condition was not eliminated by changing the outlet boundary condition however more investigation is required to prove this.

Figure 9 shows slices across the tunnel and the velocity fields throughout the tunnel for the original configuration. It can be seen that the velocity of the reversed flow near the entrance of the tunnel in the axial direction of the bars is the highest though that region is very small. The changing sign in the section near the stack indicates that there may be some vorticity at the end of the tunnel near the stack. The maximum velocity in the tunnel is about 3 m/s for this case and this occurs at the reversed flow section. Typical velocity magnitudes in the z-direction (in the direction of the bars) in the tunnel for the overwhelming majority of the tunnel flow are of the order of 0.2-0.5 m/s and there is a marked gradient in z-direction with x-coordinate (vertical direction) driven by the upwards flow of the heat.

This is confirmed in the streamline plot shown in Figure 10 which shows vorticity (swirling) about the y-axis near the entrance, swirling flow about the z-axis about two thirds of the way down the tunnel and some swirling about the x-axis at the entrance to the stack. This figure also confirms that the velocity is highest in the stack.

Figure 11 shows streamlines through the tunnel for the flat roof case. Here it can be that the axial flow through the tunnel is unidirectional with no portions of the flow leaving the tunnel rather contrary to the case of the original configuration. This indicates that the size of the stack opening at the specified locations in the tunnel is sufficient to relieve the pressure gradient setup by the difference in hydrostatic pressure. Again it is noted that the bulk of the flow is in the axial direction of the bars this is particularly true in between the bars as can be seen from the figure.

Figure 12 shows slices across the tunnel and the velocity fields throughout the tunnel for the flat roof case. It can be seen that the z- direction velocity is reversed near the first flat roof exit. The maximum velocity in the tunnel is about 6 m/s for this case and this occurs below the bars well in the tunnel. This indicates that the heat transfer regime for the flat roof case is significantly more aligned with convection forced by the hydrostatic pressure gradient than was the case for the original configuration.

The streamline plot of the entire tunnel (Figure 13) for the flat roof case shows that there exists significantly less vorticity in the bulk of the tunnel for this case than there is for the original configuration. The first flat roof induces the highest velocities below the busbar between the entrance to the tunnel and the first flat roof exit. This high velocity is beneficial for effective heat transfer and the velocity field indicates that the placement of the first flat roof exit closer to the centre may further enhance the heat transfer if needed.
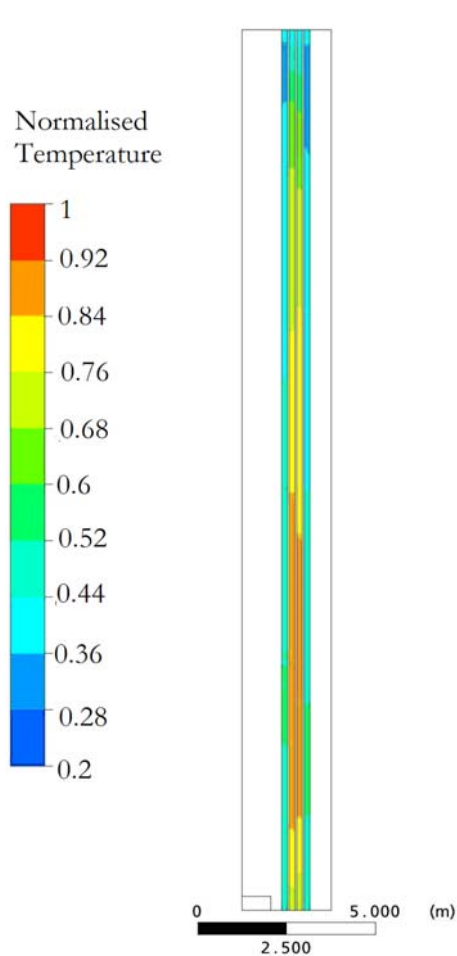
Figure 4: Normalised Temperature results along the busbar and at the inlet and exit for case 1 in table 1 (Existing Geometry and 228kA current
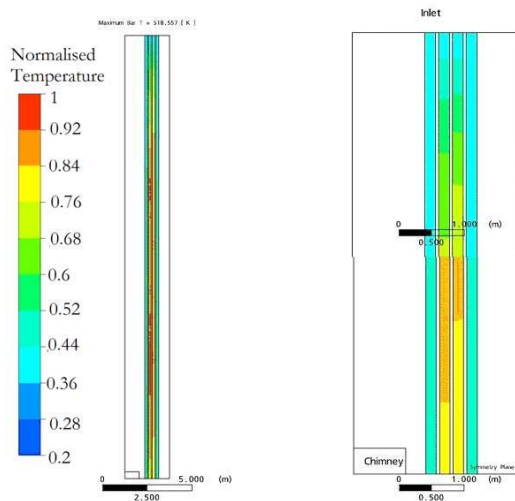

Figure 5: Normalised Temperature results along the busbar and at the inlet and exit for case 2 in table 1 (Existing Geometry and 240kA current)
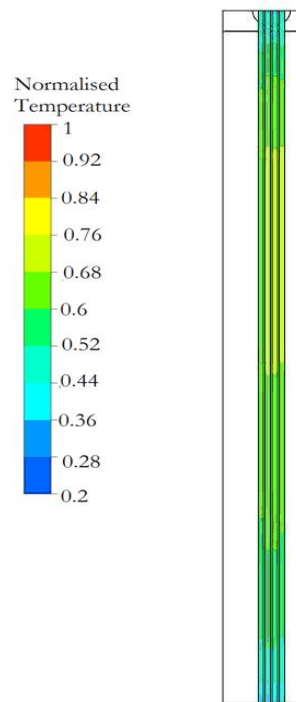

Figure 6: Normalised Temperature results along the busbar and at the inlet and exit for case 3 in table 1 (cylindrical stack geometry and 240kA current)
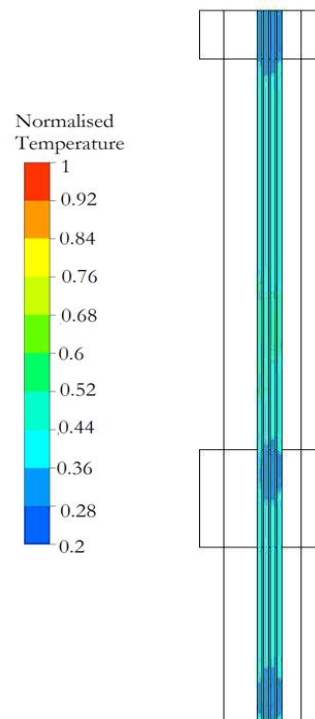

Figure 7: Temperature results along the busbar and at the inlet and exit for case 4 in table 1 (three Flat Roof Vents along the tunnel and 240kA current)

5

Figure 8: Left vector plot of velocities in the tunnel. Right close up of velocities in between and around the bars. Note positive w velocity is from the inlet to the stack.
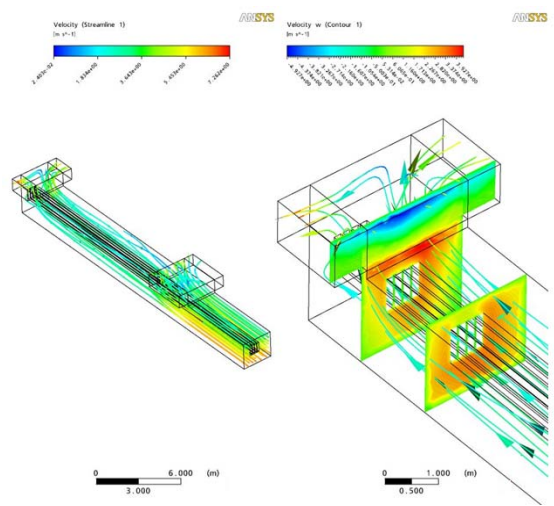

Figure 11: Left vector plot of velocities in the tunnel. Right close up of velocities in between and around the bars.
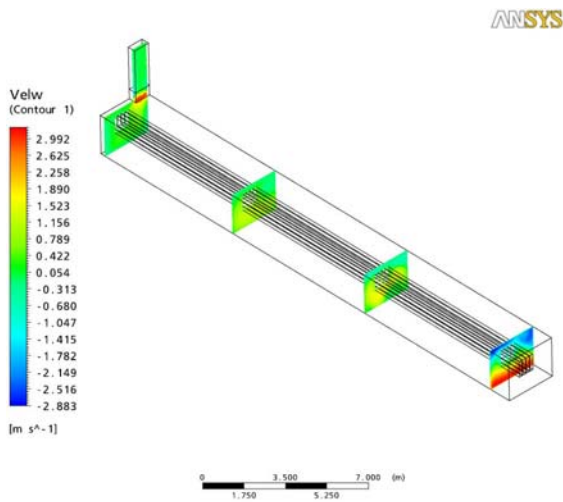

Figure 9: Cross sections showing evolutions of velocities in the axial direction. Note positive w velocity is from the inlet to the stack.
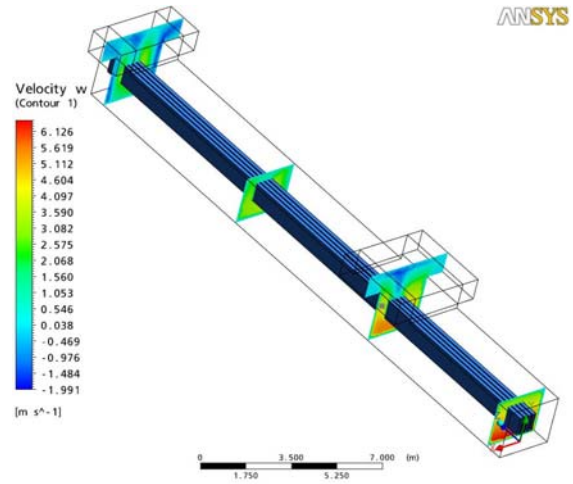

Figure 12: Cross sections showing evolutions of velocities in the axial direction.
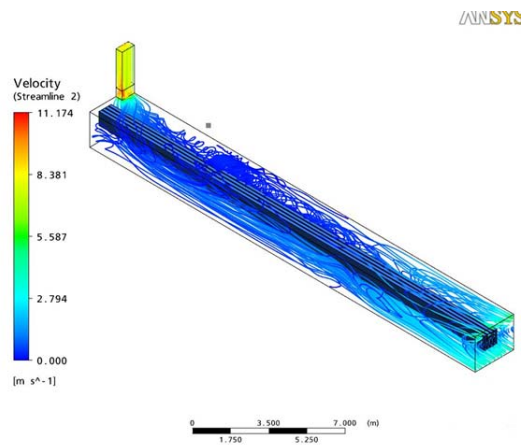

Figure 10: Streamline plot showing vorticity near the entrance and down the tube.
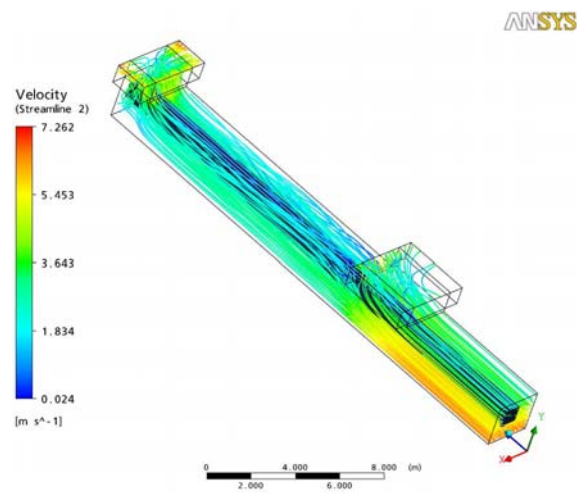

Figure 13: Streamline plot showing vorticity near the entrance and down the tube.

CONCLUSION

It is concluded that according to the cases modelled, there would exist little difference in the maximum temperatures between the 228 kA and 240 kA currents for the existing geometry. The difference exists in the portion of the busbar mass at or near this elevated temperature.

Both solutions provide significant cooling on the existing configuration and either would lower the average and maximum temperature of the bars with the Flat Roof Vent geometry clearly the most effective due to a large volumetric flow rate of air moved.

POSTSCRIPT

Tomago implemented the Flat Roofed Vent option in advance of any change in Line Current and the busbar temperatures showed an overall reduction. This was considered a highly successful result and consistent with the modelling predictions.

REFERENCES

1. ILKKA S. LAITINEN, JUHA T. TANTTU, Modelling and simulation of a copper electrolysis cell group Simulation Modelling Practice and Theory 16 (2008) 900–909
2. M. ZOLOT, K. KELLY, M. KEYSER, M. MIHALIC, A. PESARAN, A. Hieronymus, Thermal Evaluation of the Honda Insight Battery Pack (NREL/CP-540-30095), Presented at 36th Intersociety Energy Conversion Engineering Conference, 2001.
3. DEBASHIS GHOSH, PATRICK D. MAGUIRE AND DOUGLAS X. Zhu Design and CFD Simulation of a Battery Module for a Hybrid Electric Vehicle Battery Pack SAE 2009-01-1386
4. E. WIECHMANN, G. VIDAL, A. PAGLIERO, Current-source connection of electrolytic cell electrodes: an improvement for electrowinning and electrorefinery, IEEE Transactions on Industry Applications 42 (2006) 851–855.
5 INCROPERA, F.P., DEWITT, D.P., BERGMAN, T.L., LAVINE,A.S., (2006), "Fundamentals of Heat and Mass Transfer. John Wiley and Sons
6 LIDE, D. R. CRC Handbook of Chemistry and Physics. Boca Ranton, Fl.: CRC Press, 1994.